Energy Proceedings
Vol 52, 2025
ISSN 2004-2965

Numerical Simulation of Pore-Scale Supercritical CO_2 Enhanced Oil Recovery Based on Tight Sandstone Core [#]

Bingtao Yang [1], Pingchuan Dong [1*]

1 China University of Petroleum,Beijing

ABSTRACT

Carbon capture, utilization and storage (CCUS) is an important way to deal with the global climate crisis. In recent years, the geological storage of carbon dioxide has been extensively studied from micro to macro. In order to understand the percolation law of CO_2 geologic storage and EOR from the microscopic point of view, the numerical simulation of two-phase flow in conventional sandstone cores during supercritical CO_2 EOR was carried out. The two-dimensional pore structure of tight sandstone was characterized by field emission scanning electron microscopy (FE-SEM), and a two-dimensional flow model was constructed by combining Tyson polygon. The Phase field method was used to simulate the oil and gas phase flow in the process of supercritical CO_2 enhanced oil recovery. The distribution of CO_2 under different initial pressure gradients, rock wettability and viscosity ratio and the changes of oil phase saturation were compared, and the mechanism of CO_2 reservoir and percolation under the micro-three-dimensional pore scale was revealed. The results show that : (1) With the increase of the initial pressure gradient of the two phases, the fingering effect is enhanced, the spread range is reduced, the gas invasion possibility is increased, and it is possible to break through the fingering effect and realize multiple dominant channels in parallel; (2)With the increase of rock's CO_2 wettability, the spread range of CO_2 expands and the storage of CO_2 increase-es;(3)As the viscosity ratio of two phases decreases gradually, the flow resistance between fluids decreases, and the gas phase seepage capacity increases. In summary, the two-phase flow numerical simulation of CO_2 EOR based on a two-dimensional model reveals the seepage mechanism in the process of CO_2 EOR in a higher dimension, providing theoretical guidance and technical support for the study of CO_2 EOR and CO_2 geological reservoir.

Keywords: CO_2 Enhanced Oil Recovery , FE-SEM , Pore-Scale , Phase Field Method ,Numerical Simulation

1. INTRODUCTION

In recent years, the greenhouse effect caused by carbon dioxide emissions has become increasingly serious. Given the complex climate environment, reducing carbon dioxide emissions and accelerating carbon dioxide storage have become powerful means to mitigate the greenhouse effect. Carbon dioxide flooding, as an effective technology for enhanced oil recovery[1-3], has been widely studied by scholars because it allows for both carbon sequestration and emission reduction measures.

Carbon dioxide storage can be categorized into oil-bearing reservoir storage and saline aquifer storage. Oil-bearing reservoir storage involves understanding the three-phase flow behavior of oil-gas and water-water in microscopic pore throats. The underground seepage mechanism of oil-gas and water-water is complex. Additionally, tight sandstone reservoirs exhibit highly heterogeneous pore throat structures, often filled with various materials[4-12]. While the computational require-ments are relatively small, effectively evaluating the real flow characteristics of such highly heterogeneous and complex cores remains challenging [13-17]. Therefore, characterizing the complex pore throat structure of tight sandstone using scanning electron microscopy is essential[18-20].

One approach involves constructing a similar model using Tyson polygons to represent the actual two-dimensional pore throat structure[21-22]. Subsequently, the phase field method can simulate oil-oil-water three-phase carbon dioxide flooding[23-26]. This simulation provides insights into oil recovery efficiency and carbon dioxide storage efficiency under different displacement conditions, serving as a theoretical basis for designing carbon dioxide storage schemes in tight sandstone reservoirs.

This is a paper for the 16th International Conference on Applied Energy (ICAE2024), Sep. 1-5, 2024, Niigata, Japan.

2. CHARACTERIZATION OF TIGHT SANDSTONE

In this study, we utilized a field emission scanning electron microscope (FE-SEM) to examine the pores within the tight sandstone reservoir of the Bashijiqik Formation in Kuqa Shanqian, Tarim Basin. Image processing techniques were employed for threshold segmentation, pore identification, and calculation of relevant characterization parameters based on the SEM images. Our focus was on characterizing the physical properties of tight sandstone reservoirs in this specific area.

Subsequently, leveraging the reservoir characteristics, we applied the Tyson polygon method to construct a similar model. Additionally, scanning electron microscopy (SEM) was used to observe six sample groups, allowing us to analyze the pore throat structure through image analysis. We also calculated porosity and pore size distribution. The results are presented in Figure 1 and Figure 2 below.

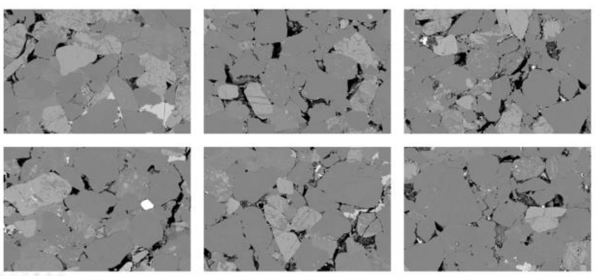

Fig. 1 FE-SEM image of tight sandstone

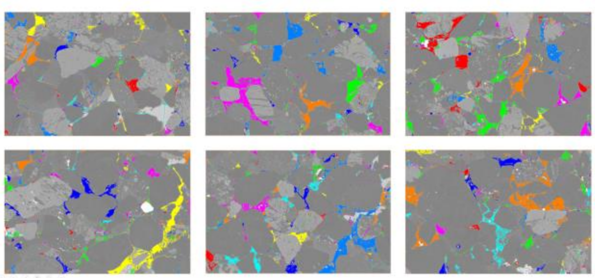

Fig. 2 Pore structure extraction

After characterization and analysis, it can be seen that the core porosity in this block ranges from 6%-11%, with a minimum of 6.84% and a maximum of 10.91%. The pore structure is dense, with pore sizes ranging from 0.5-230 μm.

The pore size distribution can be divided into three main peaks.The first peak, ranging from 0-10 μm, is primarily composed of dissolution pores within the particles and tiny pores between the particles, which account for a relatively small proportion of the pore network and are not the main oil and gas storage space.The second peak, between 10 and 100 μm, represents the intergranular throats, which constitute the main seepage channels of the tight sandstone and play a leading role in the fluid flow process.The third peak, above 100 μm, accounts for the largest proportion of the pore size distribution and is the primary space for oil and gas occurrence.

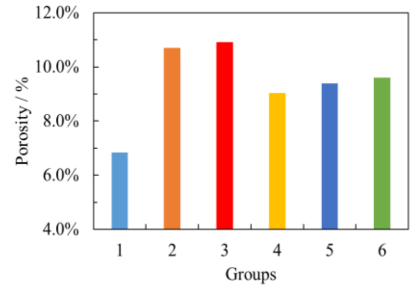

Fig. 3 Porosity distribution of tight sandstone

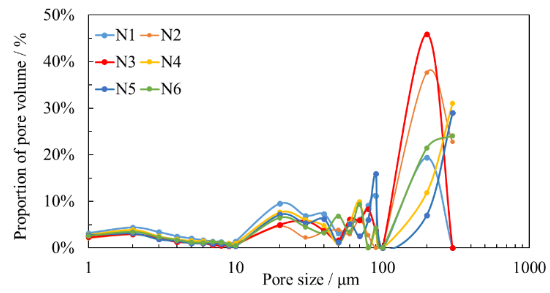

Fig. 4 Pore size distribution of tight sandstone

By characterizing the microscopic pore structure of the tight sandstone, the pore structure can be classified in detail, the main channels and locations of oil and gas flow can be analyzed, and the micro-intergranular and intra-granular pores that contribute little to the flow can be excluded.

3. PHASE FIELD METHOD AND MODELING

3.1 Theoretical basis of phase field method

The phase field method [27-28] assumes that two fluids mix in the two-phase interface region to form a diffused interface layer of a certain thickness. The movement and deformation of the interface are affected not only by convection, but also by diffusion. In this method, the physical quantities (density, viscosity, etc.) of the fluid in the homogeneous fluid phase are constant, while they change continuously in the mixed region without any jump. Similarly, the interfacial tension at the phase interface is not a sudden value, but a uniform distribution in the transition region. The phase field method solves the pressure and velocity changes of incompressible two-phase flow by coupling the continuity equation and Navier-Stokes equation [29-30]. The governing equation is as follows:

$$\rho \cdot \nabla \cdot u = 0 \tag{1}$$

$$\rho \cdot \frac{\partial u}{\partial t} + \rho \cdot (u \bullet \nabla) \cdot u = \nabla \bullet [-p + K] + F_s \tag{2}$$

$$K = \mu(\nabla u + (\nabla u)^T) \tag{3}$$

Here u represents the velocity vector in m/s; t represents time in s; ρ represents density in kg/m3; K represents the viscous force in N; σ represents the interfacial force acting on the phase interface in N/m2; μ represents viscosity in mPa·s.

The phase field equation is derived from the Cahn-Hilliard equation through the control of fluid volume conservation within the system.

$$\frac{\partial \phi}{\partial t} + u \cdot \nabla \phi = \nabla \cdot \frac{\gamma \beta}{\varepsilon^2} \cdot \nabla \cdot \psi \tag{4}$$

$$\psi = -\nabla \cdot (\varepsilon^2 \nabla \phi) + \phi(\phi^2 - 1) \tag{5}$$

The dimensionless phase field variable, ϕ, where ϕ=1 represents fluid 1, ϕ=-1 represents fluid 2, and the phase field variable continuously changes from -1 to 1 in the phase interface region. M is the migration coefficient, which represents the velocity of the phase interface under a unit driving force (i.e., chemical potential gradient). F is the mixed energy density, and N is the interface thickness. ψ is the phase field auxiliary variable.

The wettability of the fluid on the solid phase wall is determined by the following equation:

$$n \cdot \varepsilon^2 \nabla \phi = \varepsilon^2 \cos(\theta_w) |\nabla \phi| \tag{6}$$

Where n represents the unit vector normal to the solid phase surface; θ represents the solid phase surface contact angle.

3.2 Generative model

In order to analyze the supercritical CO_2-oil two-phase flow rule and oil displacement efficiency in porous media under the microscopic scale of tight sandstone, the dimensional information of the main structure of porous media channels in tight sandstone was obtained by characterizing the electron microscope images of real tight sandstone reservoirs. Combined with the image structure, a two-dimensional porous media model with similar porosity and permeability was constructed using the Tyson polygon method. This approach can effectively simulate the mineral distribution structure of tight sandstone and obtain a reasonable seepage channel. The model size is 1.5mm×1.0mm, the porosity is 10.23%, which is similar to the real sandstone structure, and the average thickness of the flow channel is 8.16μm, as shown in Figure 5.Based on the above model, the grid was divided, and the total grid number of the generated grid model was 20992.

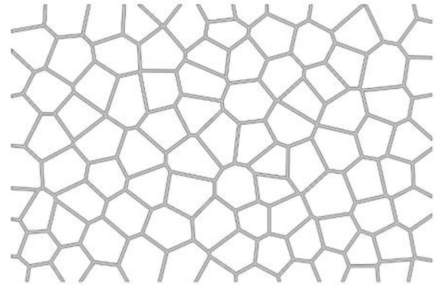

Fig. 5 Schematic diagram of a two-dimensional porous medium model

The velocity control boundary condition (constant inlet velocity and constant outlet pressure) is adopted to solve the pressure field distribution. Given the inlet velocity, a zero pressure gradient is set at the outlet, with no-slip velocity condition on the pore walls, and the pore walls have fixed wettability.

The density and viscosity of the injected supercritical CO_2 were set at 345 kg/m³ and 0.028 mPa·s, respectively, while the oil phase density and viscosity were set at 790 kg/m³ and 0.56 mPa·s, respectively. The effects of wettability, flow rate, and viscosity ratio on CO_2 displacement efficiency and CO_2 storage efficiency were investigated

4. INFLUENCING FACTORS OF CO_2 DISPLACEMEN

4.1 Wettability effect

Wettability can affect the distribution of two-phase fluid in porous structures, determine the fluid connectivity and flow capacity, and is the main control parameter that determines the fluid saturation, capillary pressure, and relative permeability. The wettability of porous media is characterized by the contact angle between the solid wall and the displacement fluid in the simulation of pore-scale two-phase flow. Due to the influence of mineral components and other factors, natural reservoirs have uneven wettability. Therefore, four sets of simulation models with different contact angles are set to reveal the seepage law in the process of supercritical CO_2 flooding under different wettability conditions. Contact angle models of 30°, 60°, 90°, and 120° were set respectively. The inlet flow rate was 0.005 m/s, the oil phase viscosity was 0.56 mPa·s, the gas phase viscosity was 0.028 mPa·s, and the viscosity ratio was 20:1.

Figure 6 shows the displacement results under different wettability conditions at 0.15 s. When the contact angle is small, the rock exhibits oleophobic characteristics, and the capillary force is the driving force of CO_2 propulsion. The CO_2 permeability is strong, the saturation increases, and the displacement interface advances at a steady and uniform speed. As the contact angle increases, the affinity between CO_2 and the rock surface gradually decreases, the capillary force gradually becomes the resistance to CO_2 migration, the CO_2 displacement route gradually breaks out, and the fingering effect becomes more pronounced. When the wetting angle is 90°, the miscible interface of the two phases of oil and gas is the smallest. At 0.05 s, CO_2 has two dominant channels, and then the two dominant channels converge at 0.15 s. With the advance of the miscible interface, CO_2 forms an obvious fingering effect at 0.25 s, and then CO_2 flows along the dominant channel, forming gas channeling, as shown in Figure 7. When the wetting angle of the rock is greater than 90°, the rock becomes lipophilic, and the capillary force becomes the displacement resistance. At this flow rate, the two-phase interface advances slowly, so the two phases gradually mix at the miscible interface, reducing the oil phase saturation and increasing the length of the miscible region. As the oil phase saturation gradually decreases, CO_2 again forms the dominant channel. The miscible region at this time is much larger than the miscible region with 0-90° wettability.

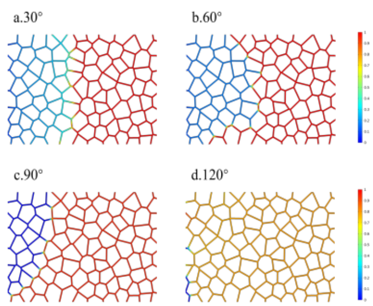

Fig. 6 CO_2 displacement interface distribution map under different wettability conditions (0.15s)

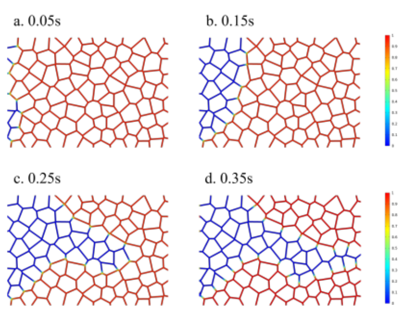

Fig. 7 CO_2 displacement interface distribution at different times (wetting Angle 90°)

The oil saturation curve at different times under different wettability (Fig. 8) was studied. It was found that when the supercritical CO_2 wettability angle is less than 90°, the remaining oil saturation will increase along with the oil recovery efficiency of CO_2 injection, and the CO_2 storage efficiency will continue to increase. Finally, the remaining oil saturation tends to plateau as the displacement front reaches the edge of the porous media, but also shows a gradually decreasing trend. The smaller the wetting angle, the lower the remaining oil saturation, the higher the oil recovery, and the higher the carbon dioxide storage efficiency.

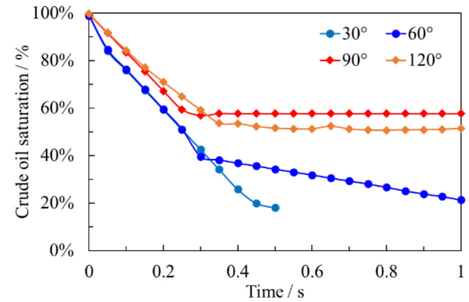

Fig. 8 Variation curve of oil saturation with time under different wettability conditions

As shown in Fig. 9, the CO_2 storage efficiency in tight sandstone reservoirs is greatly affected by rock wettability due to capillary forces, and CO_2 storage efficiency decreases significantly with the increase of CO_2 contact angle. Additionally, as depicted in Fig. 7-d, the miscible region of two-phase displacement increases significantly with the increase of contact angle.

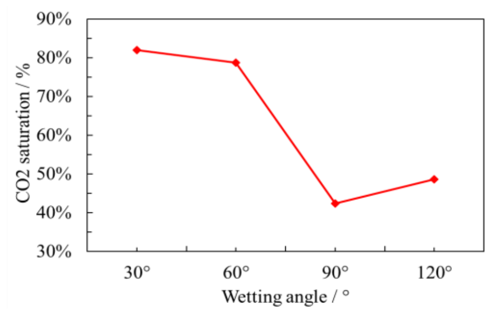

Fig. 9 CO_2 storage efficiency under different wettability conditions

4.2 Pressure gradient

In order to study the influence of pressure gradient on CO_2 storage efficiency and oil recovery in tight sandstone reservoirs, the inlet flow rate was changed to reflect the change in pressure gradient. Different injection speeds (0.001, 0.005, 0.01, 0.05, 0.1 m/s) were set to simulate displacement and storage laws under varying pressure gradients. Figure 10 shows the CO_2-oil two-phase distribution from CO_2 displacement to breakthrough under different injection rates.

When the injection rate is low, the channeling effect is relatively weak, and the CO_2 displacement front advances uniformly at first, then forms a wide dominant channel. As the injection speed increases, the channeling effect of the displacement fluid is enhanced, and it is easier to form dominant channels. After the dominant channels form, the oil recovery efficiency and CO_2 storage efficiency gradually stabilize, but the storage efficiency decreases from 61.62% to 42.40%. As the injection rate continues to increase, the fingering effect becomes more pronounced. At this point, the oil recovery efficiency and CO_2 storage efficiency continue to decrease, but the change is small.

When the injection speed reaches 0.05 m/s, the original dominant channels are broken through, and two obvious dominant channels are formed, increasing the total swept area. As a result, the oil recovery efficiency and CO_2 storage efficiency increase from 40.05% to 49.92%. Further increasing the injection rate causes the dominant channel to become singular again, but the increased flow rate expands the spread range of CO_2, improves its seepage capacity, and enables CO_2 to enter channels that were not easily accessible, thereby improving CO_2 storage efficiency.

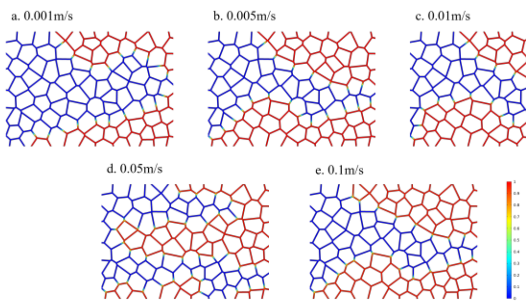

Fig. 10 CO_2 displacement interface distribution at different injection rates

As shown in Figure 11, when the CO_2 injection rate is low, the swept area is large, and the fingering effect is weak, but the seepage rate is slow, affecting crude oil production. The injection rate needs to exceed a certain critical value for the fingering effect to increase the seepage capacity of CO_2, thereby improving oil recovery and CO_2 storage efficiency. Therefore, it is necessary to carefully select the optimal injection speed for actual production, as this can greatly improve oil recovery efficiency and CO_2 storage efficiency.

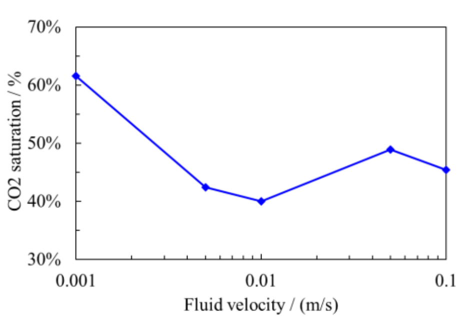

Fig. 11 CO_2 storage efficiency under different injection rates

4.3 Viscosity ratios

The viscosity of supercritical CO_2 varies significantly under the influence of temperature and pressure, resulting in different CO_2 viscosity values at different reservoir depths. To study the CO_2 displacement distribution under various reservoir conditions, 5 groups of flow models with different viscosity ratios (1:20, 1:10, 1:5, 1:2, and 1:1) were set up. This allowed the researchers to obtain the CO_2-oil two-phase distribution from CO_2 displacement to breakthrough, as shown in FIG. 12.

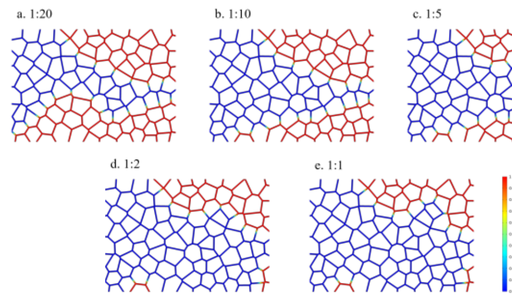

Fig. 12 CO_2 displacement interface distribution under different viscosity ratios

When the viscosity ratio is 1:20, the pointing effect is obvious, and the CO_2 saturation is low when the displacement breakthrough occurs, with CO_2 forming a narrow seepage channel. As the viscosity ratio is increased to 1:5, the pointing effect is significantly weakened and the fluid sweep range becomes wider. When the viscosity ratio is further increased to more than 1:2, the dominant channels are completely connected, forming a large miscible region, resulting in a higher CO_2 storage rate and more adequate displacement.

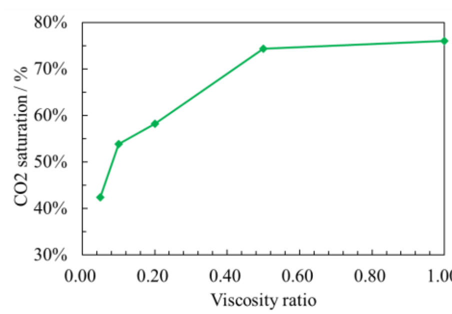

Fig. 13 CO_2 storage efficiency under different viscosity ratios

As shown in Figure 13, when the viscosity is relatively low, an appropriate increase in the viscosity ratio can greatly expand the swept area of CO_2 and facilitate its flow, thereby achieving a better storage effect.

5. INFLUENCING FACTORS OF CO_2 DISPLACEMEN

1. The phase field method can effectively track the interfacial changes in two-phase flow processes and

characterize the fluid percolation process dominated by capillary forces in tight sandstone reservoirs. This is an effective method to study multiphase flow in porous media at the micro-pore scale. The two-dimensional porous media two-phase flow model based on Tyson polygon can effectively simulate the fluid flow in tight sandstone reservoir cores and significantly reduce calculation time. Combined with scanning electron microscope image processing results, the model can simulate the actual core porosity and aperture parameters, and analyze the flow pattern and phase interface effects in the two-dimensional model.

2.As the wettability of the rock to CO_2 increases, the fluid displacement gradually changes from finger-like to piston-like, with a wider spread range and improved continuity of the fluid channel, resulting in greatly increased oil displacement efficiency. The effect of the CO_2 injection rate on the phase interface during displacement is significant. Due to the influence of capillary forces, a lower CO_2 injection rate can achieve a larger sweep range, but it also reduces crude oil production. With increasing injection speed, the oil recovery efficiency and CO_2 storage efficiency first decrease and then increase. When the pressure gradient effect gradually exceeds the capillary force effect, increasing the injection fluid speed has a positive impact on oil recovery efficiency and CO_2 storage efficiency. The smaller the viscosity difference between the two phases, the lower the flow resistance between the phases, leading to more effective displacement, which is beneficial for improving the seepage capacity of CO_2 and thereby enhancing CO_2 storage efficiency.

3.The percolation process of CO_2 geological storage in the porous media of tight sandstone was revealed at the microscopic scale, providing a basic explanation for the study of CO_2 percolation at the macroscopic scale and offering a theoretical basis and technical support for improving the oil recovery efficiency of tight sandstone reservoirs and the efficiency of CO_2 geological storage.

REFERENCE

[1] Li Q, Cai B, Chen F, et al. Review of environmental risk assessment methods for carbon dioxide geological storage[J]. Environmental Engineering, 2019, 37(2): 13-21.

[2] Edwards R W J, Celia M A, Bandilla K W, et al. A model to estimate carbon dioxide injectivity and storage capacity for geological sequestration in shale gas wells[J]. Environmental science & technology, 2015, 49(15): 9222-9229.

[3] Espinoza D N, Kim S H, Santamarina J C. CO 2 geological storage—Geotechnical implications[J]. KSCE Journal of Civil Engineering, 2011, 15: 707-719.

[4] Anderson S, Newell R. Prospects for carbon capture and storage technologies[J]. Annu. Rev. Environ. Resour., 2004, 29(1): 109-142.

[5] Luo J, Xie Y, Hou M Z, et al. Advances in subsea carbon dioxide utilization and storage[J]. Energy Reviews, 2023, 2(1): 100016.

[6] Jiahao H A O, Yunkai Y U E, Jiajun ZHANG J Y, et al. Research status and development prospect of carbon dioxide energy-storage technology[J]. Energy storage science and technology, 2022, 11(10): 3285.

[7] Raad S M J, Hassanzadeh H. Prospect for storage of impure carbon dioxide streams in deep saline aquifers—A convective dissolution perspective[J]. International Journal of Greenhouse Gas Control, 2017, 63: 350-355.

[8] Ku H, Miao Y, Wang Y, et al. Frontier science and challenges on offshore carbon storage[J]. Frontiers of Environmental Science & Engineering, 2023, 17(7): 80.

[9] Junjia F, Haimin Z, Shaobo L. Pore structure and gas migration characterization of tight sandstone in Kuqa depression of Tarim basin[J]. Journal of University of Chinese Academy of Sciences, 2014, 31(1): 108.

[10] Sun L H, Xiao H M, Tan L, et al. Pore structure comparison and difference mechanism between tight sandstone and tight conglomerate reservoirs[J]. Acta Geologica Sinica, 2022, 96(6): 2155-2172.

[11] Lai J, Wang G, Wang Z, et al. A review on pore structure characterization in tight sandstones[J]. Earth-Science Reviews, 2018, 177: 436-457.

[12] Wei W, Yuanjuan S, Jing H, et al. Fractal characteristics of pore-throat structure in tight sandstones using high-pressure mercury intrusion porosimetry[J]. 2021, 40(4): 22-30, 48.

[13] Wu F, Yao C, Cong L, et al. Pore-scale gas–water flow in rock: Visualization experiment and simulation[J]. Open Geosciences, 2020, 12(1): 532-546.

[14] Liu Q, Li J, Liang B, et al. Microscopic flow of CO_2 in complex pore structures: A recent 10-year review[J]. Sustainability, 2023, 15(17): 12959.

[15] Lan R E N, Yanming F U, Yongquan H U, et al. Simulation of Microscopic gas flowing in shale based on LBM[J]. Special Oil & Gas Reservoirs, 2017, 24(3): 70-75.

[16] Liu J, Wang Y, Song R. A pore scale flow simulation of reconstructed model based on the micro seepage experiment[J]. Geofluids, 2017, 2017(1): 7459346.

[17] Liang Z, Wang C, Zhou Y. Analysis of seepage characteristics of complex pore structure rock by digital core method[J]. Chemistry and Technology of Fuels and Oils, 2020, 55(6): 756-764.

[18] Klaver J, Desbois G, Littke R, et al. BIB-SEM pore characterization of mature and post mature Posidonia Shale samples from the Hils area, Germany[J]. International Journal of Coal Geology, 2016, 158: 78-89.
[19] Li W, Lu S, Wang M, et al. Quantitative characterization of micro heterogeneity of tight reservoirs by large-view FE-SEM Msplicing technology[J]. Oil Gas Geol, 2022, 43(6): 1497-1504.
[20] Songtao W, Rukai Z, Xun L, et al. Evaluation and application of porous structure characterization technologies in unconventional tight reservoirs[J]. Earth Science Frontiers, 2018, 25(2): 191.
[21] Han D, Bray M. Automated Thiessen polygon generation[J]. Water resources research, 2006, 42(11).
[22] Mochnacki B, Ciesielski M. Micro/macro model of solidification. Numerical simulation using the control volume method[C]//17th International Conference on Computer Methods in Mechanics CMM-2007, CD-ROM Proceedings, Łódź-Spała. 2007.
[23] Meng Q, Zhao L, Li P, et al. Experiments and phase-field simulation of counter-current imbibition in porous media with different pore structure[J]. Journal of Hydrology, 2022, 608: 127670.
[24] Li H, Wang F, Wang Y, et al. Phase-field modeling of coupled reactive transport and pore structure evolution due to mineral dissolution in porous media[J]. Journal of Hydrology, 2023, 619: 129363.
[25] Younes N, Wautier A, Wan R, et al. DEM-LBM coupling for partially saturated granular assemblies[J]. Computers and Geotechnics, 2023, 162: 105677.
[26] Gao H, Abdullah H, Tatomir A B, et al. Pore-scale study of the effects of grain size on the capillary-associated interfacial area during primary drainage[J]. Journal of Hydrology, 2024, 632: 130865.
[27] Moelans N, Blanpain B, Wollants P. An introduction to phase-field modeling of microstructure evolution[J]. Calphad, 2008, 32(2): 268-294.
[28] Cahn J W, Hilliard J E. Free energy of a nonuniform system. I. Interfacial free energy[J]. The Journal of chemical physics, 1958, 28(2): 258-267.
[29] Langer J S. Models of pattern formation in first-order phase transitions[M]//Directions in condensed matter physics: Memorial volume in honor of shang-keng ma. 1986: 165-186.
[30] Hohenberg P C, Halperin B I. Theory of dynamic critical phenomena[J]. Reviews of Modern Physics, 1977, 49(3): 435.